Institute of Space and Aeronautical Science, University of Tokyo
Report No. 394, January 1965

Experimental Studies in a Low Density Gun Tunnel Stream

By

Hakuro OGUCHI, Hiroki HONMA and Katsushi FUNABIKI

Summary: First the flow survey is made for the low-density hypersonic flow, which is achieved by a low-density operation of the gun tunnel (or free piston compression). In particular the measurements of flow velocity and, hence, of stagnation temperature are worked out by means of an explosion-wire technique and the flow survey done by traversing a free molecule calorimeter in the test flow region. With these diagnostics the characteristic feature of the test flow is investigated. It is found that, by a low-density operation of the present gun tunnel, the test flow of Mach number 10 and Reynolds number 650 (per cm) is achieved, which is applicable to experimental studies on low-density hypersonic flow problems.

Secondly an experimental study is made concerning the shock-layer structure ahead of a sphere in a low-density hypersonic flow, achieved by the present gun tunnel. The scanning-electron-beam densitometer is developed to obtain a density distribution along a scanning path of the beam during one shot of the gun tunnel. By means of this device the density distribution across the shock layer is measured for a sphere of 12.4 mm in radius, in which case the Reynolds Re_∞ is about 800. The present data exhibit a qualitative agreement with Levinsky-Yoshihara profile which was computed for argon flow of Mach number $M = 10$ and $Re_\infty = 10^3$ and 10^2.

I. INTRODUCTION

A free piston compression hypersonic wind tunnel is known as "hypersonic gun tunnel". In this device, a piston is propelled down a tube by the pressure of a driver gas. The test gas ahead of a piston is used after compression as the working fluid for a hypersonic wind tunnel. The hypersonic wind tunnel requires a source of air at sufficiently high temperature and pressure. Therefore, for an ordinary operation of the gun tunnel, the initial pressure of gas in the tube or barrel must be high enough to produce a gas at sufficiently high pressure by the free piston compression. The gun tunnel is rather similar to the shock tunnel, in which the shock-wave compression is applied instead of the free piston compression. However the gun tunnel has a remarkable merit in a comparatively longer flow duration.

For a low-density high-speed flow, a source of gas must be at high temperature but at low pressure. This requirement will be met by the gun tunnel if the gas is initially charged in the barrel at a pressure comparatively lower than for the ordinary operation. In general most of the probe measurements in a low

density flow need a longer flow duration. For a low-density flow, therefore the gun tunnel is much more preferable compared with the shock tunnel so long as the flow duration is concerned. However, the flow duration of gun tunnel is still not sufficiently long to apply most of techniques established in a low-density tunnel.

In the present experiment, first some of diagnostics have been developed for a short-duration low-density hypersonic flow achieved by the gun tunnel. These are the flow velocity measurement by means of an explosion wire technique, the flow survey by means of a free molecule calorimeter and the density-distribution measurement by means of a scanning-electron-beam densitometer. The densitometer has been designed in such a way that the electron beam emitted from the electron gun can be scanned in parallel with the lens axis. A period of the beam scanning is much less than the flow duration, so that the density distribution along the scanning line can be obtained on the detector plate during one shot of the gun tunnel. With these diagnostics it is found that the test flow of Mach number 10 and Reynolds number 650 (per cm) is achieved for air by an appropriate operation of the present gun tunnel.

Secondly, an experimental study is made concerning the shock-layer structure ahead of a sphere in a low-density hypersonic flow, achieved by the gun tunnel. The density distribution along the stagnation line across the shock layer has been measured by means of the scanning-electron-beam densitometer. The measurements have been made for case of the Reynolds number about 800, based on the sphere radius. Finally a comparison of the present data with the theoretical results will be discussed.

II. Low-Density Gun Tunnel and Flow Velocity Measurement*

This tunnel (Figure 1) consists mainly of a high-pressure vessel and a barrel connected to a conical nozzle, followed by a cylindrical test chamber and a vacuum vessel. The illustrative sketch is shown in Figure 2. The dimensions of major components are as follows:

High pressure vessel; 80 cm long section of 70 mm in. dia.,

Barrel; 3 m long tube of 50 mm smooth bore.

Both high pressure vessel and barrel are installed on a carriage which can be electrically drived along a rail.

Diaphragm; a sheet of thin cellophane which can be burst by a mechanical plunger.

Nozzle diaphragm; a sheet of thin cellophane which bursts on the arrival of the shock wave.

Nozzle; 16 deg (total angle) conical nozzle expanding from a 2 mm dia. throat to a 170 mm dia. exit. The flow is ejected into a 500 mm dia. cylindrical test chamber of 600 cm in length, as a free jet.

* The works involved in Sections II and III have been done mainly by the first and third authors, based on the previous preliminary work [1].

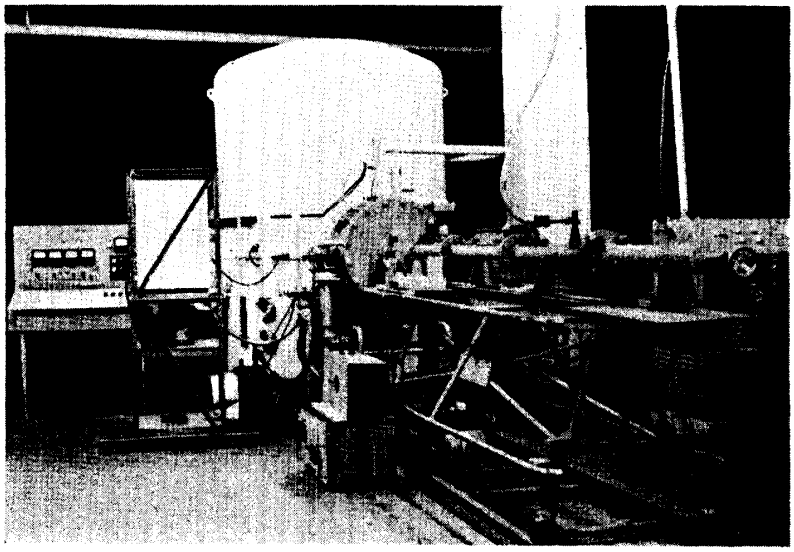

FIGURE 1. Low-density gun tunnel.

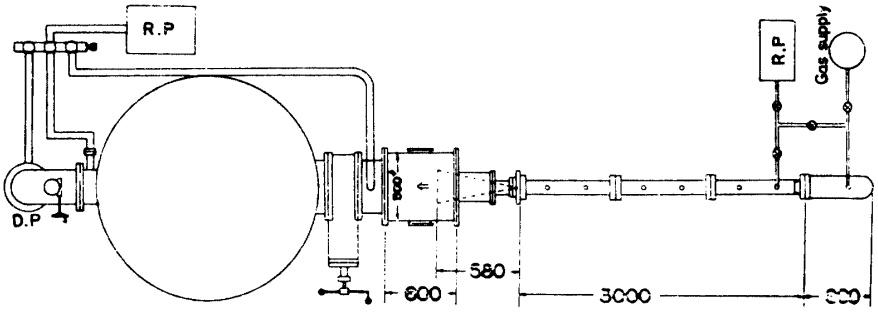

FIGURE 2. Assembly of gun tunnel (nnmbers in mm).

Vacuum vessel; 5 m^3 in capacity, evacuated down to a pressure of about 10^{-4} mmHg before run, by the series operation of rotary pump and oil diffusion pump.

One of appropriate running conditions has been determined after many preliminary runs by using air as a test gas. The initial pressure at the high pressure vessel is about 1.7 $kg/cm^2.g$ and the pressure at the barrel 15 mmHg. For each run an alminium piston of about 17.5 gr in weight was used. The speed of piston was measured by introducing to the electric counter the signals which are produced from contacts of the piston with the two electric leads mounted near the end of barrel in 20 cm distance. The average speed was about 200 m/sec under the present operation.

The diaphragm-type pressure gage was installed at the end of barrel and the output was displayed on the oscilloscope. One of the typical records is shown in Figure 3, with a free-molecule calorimeter record which will be illustrated later. The measurement for the barrel pressure shows that the period of time available for the experiment, in which the pressure is nearly constant, is about 50 msec or more. After a steep overshoot at the initial stage, the pressure is nearly constant but it indicates a slow fluctuation according to the piston motion.

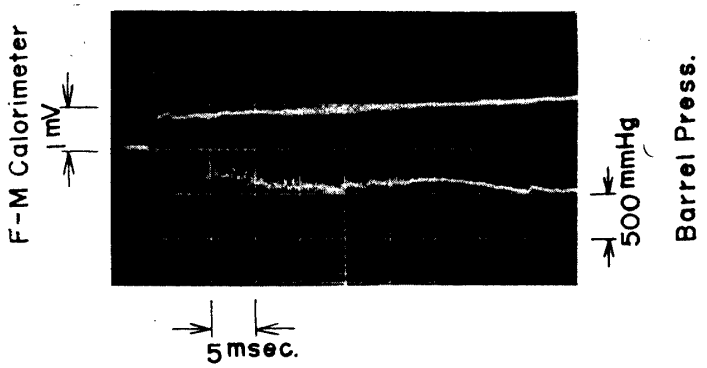

FIGURE 3. Pressure at barrel end and free-molecule heat transfer to a wire.

However it will be later shown from the flow survey at the test section that the test flow condition undergoes no appreciable effect from such a fluctuation of barrel pressure.

The stagnation temperature was estimated from the velocity measured at the test section. The flow velocity is very high so that the stagnation temperature T_0 is given by

$$T_0 \approx \frac{1}{2C_p} u_\infty^2 \qquad (1)$$

where u_∞ is the velocity at the test section and C_p the specific heat. The flow velocity was measured by tracking the radiant medium which is produced by the explosion of a thin platinum wire (20 micron dia. and 10 mm in length). The electric energy charged up to 100 V in the condenser of 10^3 μF is instantly released through a platinum wire and a mercury switch, which is adjusted to contact of an appropriate instance after the flow start by an imposed delay circuit. The pictures of explosion process were taken by a 16 mm high speed camera (max. 10^4 pictures per sec). A part of pictures is shown in Figure 4.** It can be expected from these pictures that the radiant medium appears to follow the flow. The two photomultipliers were used as "time of arrival" gages, in which case the optical system is arranged as shown in Figure 5. The outputs were displayed on a dual-beam oscilloscope, a record being shown in Figure 6. This record was for the case when the wire explosion was ignited after about 6 msec from the flow start. Since the stagnation temperature and thus the flow velocity are not always constant during the flow running, its time-dependence has been examined by exploding the wire at the instances of 10, 20, 30 and 40 msec from the flow start. It was found from the results of several runs that the flow velocity and hence stagnation temperature indicate no appreciable decrease during the time from the flow start to about 30 msec. On average

** Note that the splitted wires flow away downstream after the extinguishment of the gas discharge. Also note that there exists a bright region ahead of a sphere, which may be considered "shock layer", its thickness being at a consistent agreement with that obtained by an electron-beam densitometer.

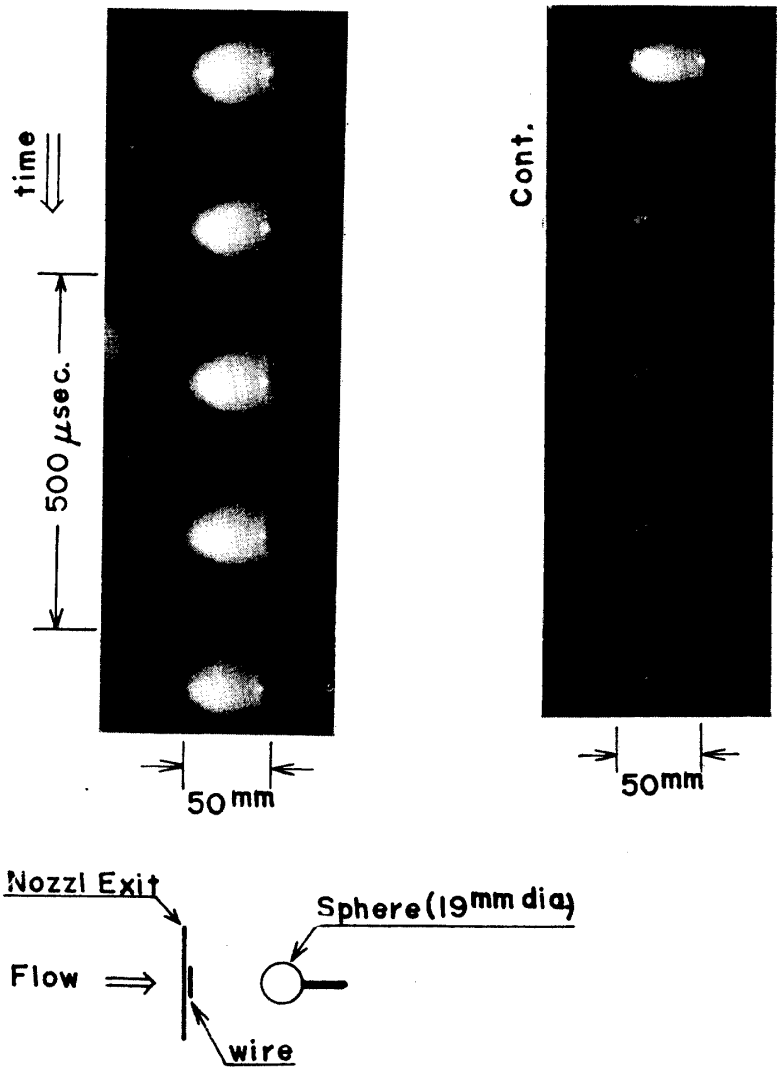

FIGURE 4. High-speed camera record of the thin wire explosion in the test flow.

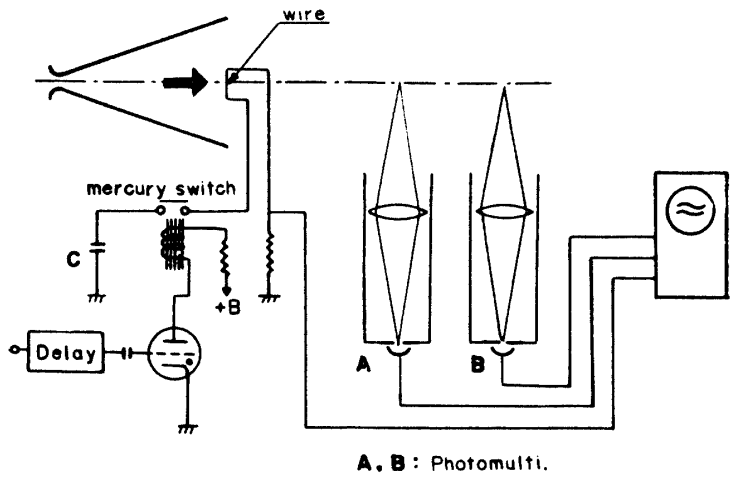

FIGURE 5. Arrangement of optical system for the velocity measurement.

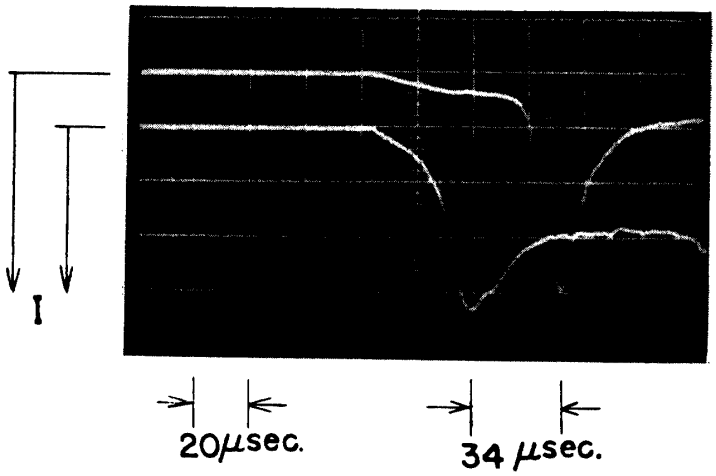

FIGURE 6. Photomultiplier records for the velocity measurement.

over this period of time, the flow velocity was about 1350 m/sec and the stagnation temperature about 1,000°K, under the present operation of the gun tunnel. In comparison with the characteristics of the ordinary gun tunnel stream [2], the stagnation temperature decrease with time appears to be slower while the temperature slightly lower.

III. Survey of Test Flow by Free Molecule Heat Transfer Probe

For the measurement of free molecule heat transfer, a thin platinum wire (20 micron dia.) was used as a calorimeter. The wire is thin enough to be in a free molecule condition, while it has a heat capacity large enough to act as a calorimeter or heat storage in a period of test time.

The local free molecule heat transfer rate q_{FM} to the surface whose element makes the angle θ with the free stream velocity vector, is given when the speed ratio is very large as follows [3]:

$$q_{FM}=\frac{1}{2}\beta\rho_\infty u_\infty^3 \sin\theta\left[1-\frac{1}{2}\frac{\gamma+1}{\gamma-1}\frac{T_b}{T_\infty}\frac{1}{\mathcal{S}^2}\right] \qquad (2)$$

where ρ_∞ is the free-stream density, u_∞ the free-stream velocity, $\mathcal{S}$ the speed ratio, β the accommodation coefficient, γ the specific heat ratio and T_b/T_∞ the temperature ratio of the surface to the free stream. If the heat transfer to the shadow region from the free stream is neglected, the total heat transfer q_{total} can be obtained by the integration of Eq. (2), that is

$$q_{total}=\frac{1}{2}\beta\rho_\infty u_\infty^3 S\left[1-\frac{1}{2}\frac{\gamma+1}{\gamma-1}\frac{T_b}{T_\infty}\frac{1}{\mathcal{S}^2}\right] \qquad (3)$$

where S is the frontal area of a cylinder.

Since the wire has a heat capacity large enough to act as a heat sink during

a period of test time, the heat balance concerning the wire is expressed as†

$$(C_p\rho V)_{wire}\frac{d\bar{T}}{dt}=q_{total}$$

where $\bar{T}$ is the mean temperature of the wire and V the volume of the wire, and $(\quad)_{wire}$ denotes quantities pertinent to the wire. By the use of a bridge circuit shown in Figure 7a, the voltage output E is related to the electric resistivity of the wire and hence to the temperature $\bar{T}$. Therefore the total heat transfer q_{total} to the wire can be expressed in terms of E, as follows:

$$q_{total}=\left(\frac{C_p\rho V}{\alpha}\right)_{wire}\frac{2}{E_0}\frac{dE}{dt} \tag{4}$$

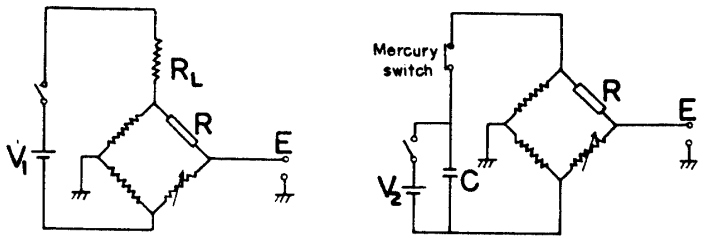

a

E = voltage output
R = calorimeter
R_L = 2000 ohm
V_1 = 50 v

b

C = 1000 μF
V_2 = 12 v

FIGURE 7. Bridge circuits for heat-transfer measurement and calibration.

where α is the resistivity coefficient of the wire and E_0 the voltage applied to the calorimeter. One of the typical records obtained at the center of test chamber is shown in Figure 3 and plotted in Figure 8. The voltage output E increases linearly with time. By the use of Eq. (4) the total heat transfer to the wire can be obtained from the slope of the voltage output. The constancy of the slope assures that the flow condition is held unchanged during the period of test time.

The quantity $(C_p\rho V/\alpha)_{wire}$ was determined by the use of the calibration circuit similar to that for a thin film thermometer [4] (Figure 7b). The heat input Q in cal/sec is given by

$$Q=\frac{i_1^2R_1}{4.19}$$

Since, for that case, the voltage output is given by the relation similar to Eq. (4), we obtain

† The heat loss from the wire ends may be neglected, because the concerning period of time is short.

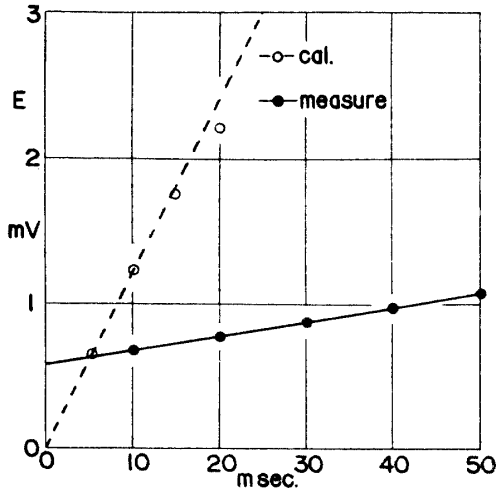

FIGURE 8. Voltage output E of a calorimeter versus time.

$$\left(\frac{C_p\rho V}{\alpha}\right)_{wire} = \frac{i_1^2 R_1}{8.38}\,\frac{E_0}{dE/dt} \qquad (5)$$

The voltage output displayed on the oscilloscope is shown in Figure 9 and plotted against time in Figure 8. The quantity $(C_p\rho V/\alpha)_{wire}$ was thus determined from the slope of the voltage output E.

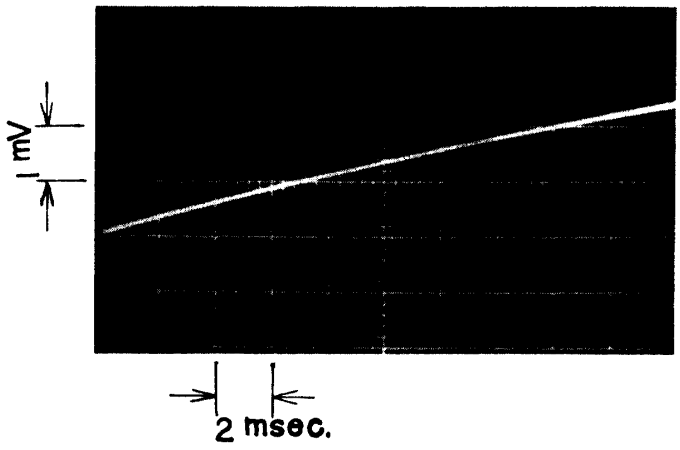

FIGURE 9. Oscilloscope record of voltage output for the calibration of a calorimeter.

The total heat transfer to the wire was measured along the axis of the test chamber from the nozzle exit towards downstream. The results are shown in Figure 10, in which the heat transfer is referred to that at the center of test chamber. The measurement was also done along the line normal to the axis at the center of test section. The results are shown in Figure 11. As can be seen from Eq. (3) the total heat transfer should be the same for the same flow condition. From Figure 11, therefore the test flow appears to have a fairly distinct core, within which the flow is nearly uniform. The diameter of

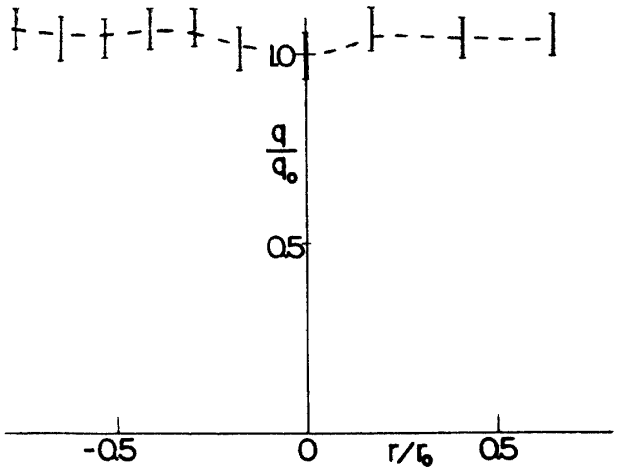

FIGURE 10. Ratio of free-molecule heat transfer rate to that at the center of test chamber, q/q_0 along the flow axis (r is measured from the nozzle exit and r_0 the radius of nozzle).

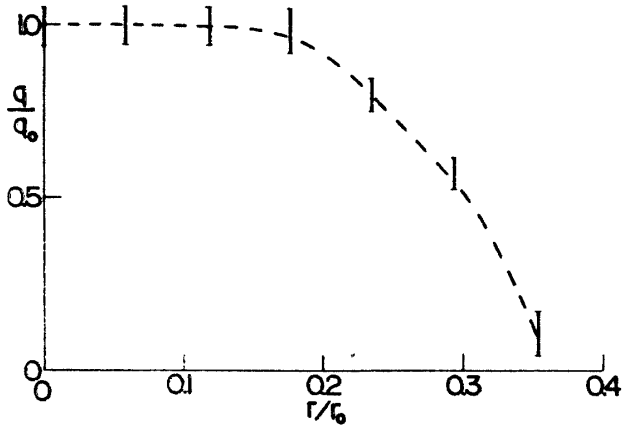

FIGURE 11. Ratio of free-molecule heat transfer rate to that at the center of test chamber, q/q_0 along the normal to the axis at the center (r is measured from the center and r_0 the radius of nozzle).

this core is roughly estimated about 50 mm at the center of the test section.

As was mentioned in the preceding section, the stagnation pressure and temperature have already been measured. Furthermore the density at the test section can be obtained from the shock-layer density measurements by means of the electron-beam densitometer, on which a detailed description will be provided later in the succeeding section. From these experimental data, the flow Mach number or Speed ratio can be determined. For the present operation the characteristic parameters of the test flow, thus determined are as follows:

Mach number; $M \approx 10$

Reynolds number; $Re_\infty \equiv \rho_\infty u_\infty R_b / \mu_\infty \approx 650 R_b$

where μ_∞ is the viscosity coefficient for the free stream. We thus see that a

hypersonic flow appropriate to investigate arodynamics in transitional regime is achieved by the present low-density gun tunnel.

Since the surface temperature T_b is assumed to be the room temperature, in Eq. (3) the accommodation coefficient β is only the unknown. In principle, therefore the free-molecule heat transfer measurements will provide a quantitative knowledge about the accommodation coefficient. Since, however, the accommodation coefficient depends on not only the wire material but also surface cleanness, the absolute measurement of the free-molecule heat transfer will require a further extensive study.

IV. Scanning-electron-beam Densitometer††

In this section the electron-beam densitometer will be described, which is designed in such a way that a beam can be scanned in parallel with the lens axis across a test flow in a period of time shorter than the flow duration. This device consists mainly of an electron gun, electric lens system and detector. The picture of the device is shown in Figure 12. The electron gun of a com-

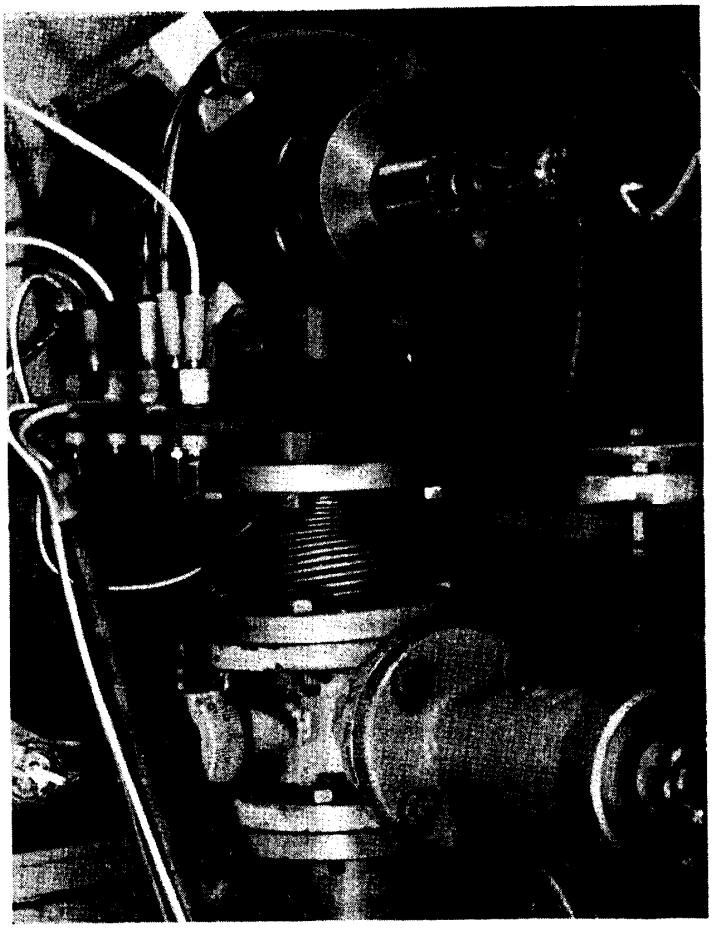

FIGURE 12. Scanning-electron-beam densitometer (demountable electron gun and its associated vacuum system).

†† The works involved in Sections IV and V have been done mainly by the first and second authors.

mercial TV tube was used, in which the oxide cathode was replaced by a tungsten cathode. In the lens system a first deflector, a slit, a second deflector and a collimator are aligned along the lens axis. The lens system was designed by the Technical Research Laboratories, Nihon Hōsō Kyōkai (Japan Broadcasting Corporation). The cross section of a collimator§ is rectangular, its longer edge being about 70 mm. The scanning beam was checked to be collimated for the path within about 25 mm from the axis. The electron gun and lens system are installed on one side of the test chamber, and the phosphor P 16 detector and a photomultiplier 7696 are on the opposite side (see Figure 13). The distance of the detector from the aperture (0.3 mm dia.) is 63.8 cm. A beam spot projected on the detector plate was about 0.5 mm wide in the scanning direction. The beam was scanned by the supply of a saw-tooth-type voltage for the first deflector. The output of the pressure transducer at the end of barrel was applied as the triggering signal to the voltage supply circuit.

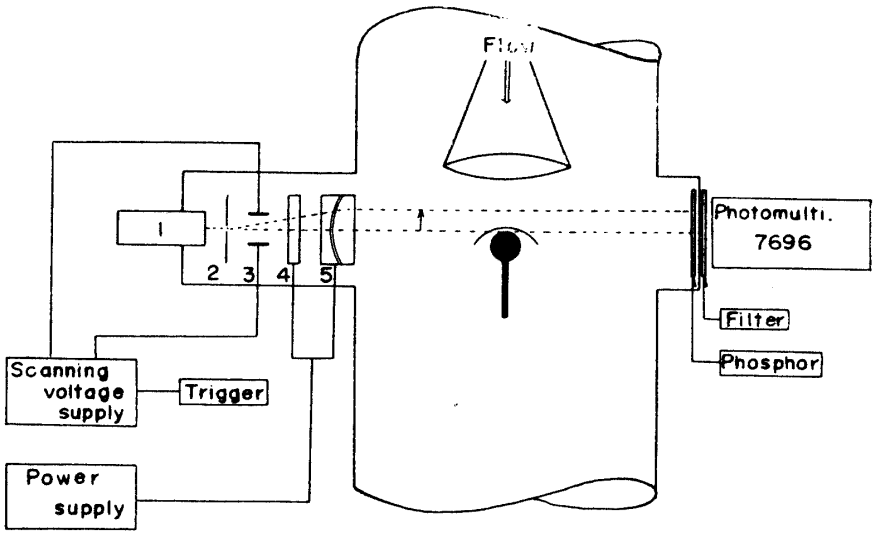

FIGURE 13. Schematic diagram of scanning-electron-beam densitometer.
1: Electron gun, 2: Aperture, 3: First deflector
4: Second deflector, 5: Collimator

The beam runs off the axis when the antisymmetric excess voltage is statically supplied to both plates of the first deflector. For that case the beam direction was determined by traversing an opaque body on a plane normal to the axis of lens system at the center of test chamber. The applied traverse mechanism installed on the base of test chamber is shown in Figure 14. It was thus checked that the beam is always collimated in the direction of axis of lens system.

As is well known, the electron beam decays when the beam runs through a gas medium, air for the present experiment, due to the electron-atom (or -molecule) collisions. For a given accelerating potential of the electron beam, the ratio of the intensity I to the initial I_0 depends both on the mean density $\bar{\rho}$ of gas along the beam path and on the path length L. That is,

§ The reader should refer to Japanese Utility Model Gazette no. 1961-18128.

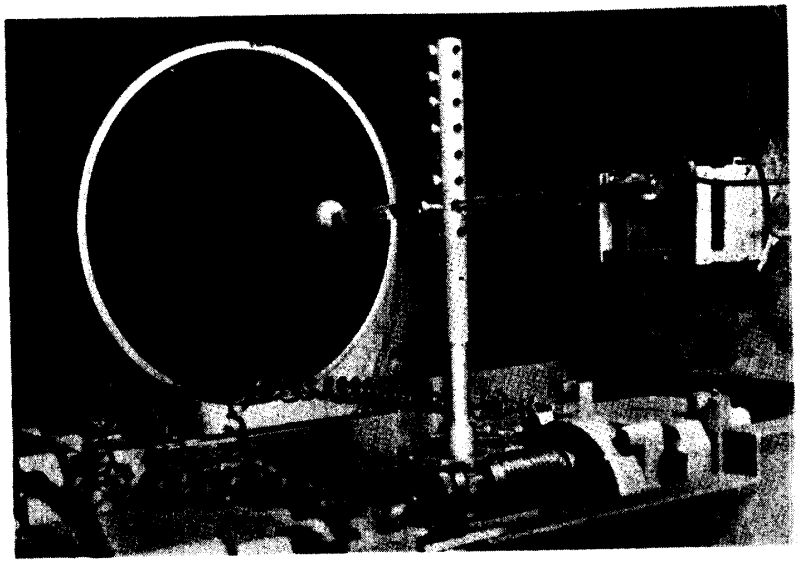

FIGURE 14. Inside view of test chamber (Nozzle exit, collimator of the electric lens and traverse mechanism).

$$I/I_o = f(\bar{\rho}L)$$

In our device the accelerating potential was 3 KV and the path length about 63.8 cm. The intensity ratio I/I_0 is plotted against $\bar{\rho}/\rho_0$ where ρ_0 is the density of air at NTP, in Figure 15.

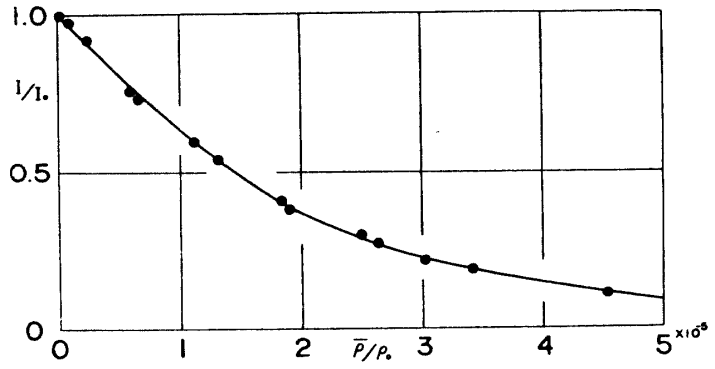

FIGURE 15. Intensity ratio I/I_0 versus density ratio ρ/ρ_0 (for air, accelerating potential 3 KV and beam path length 63.8 cm).

Evidently this relation holds regardless of whether a beam is fixed or scanned. With respect to this point, the scanning electron beam densitometer is essentially the same as the fixed beam densitometer, which was successfully used for the low-density-flow experiments (for example, see [5], [6], [7], References cited there and [8]).

V. Density Measurements for the Shock Layer Ahead of a Sphere

In this section the shock layer ahead of a sphere and, in particular, the

density distribution across the layer are investigated by means of the scanning-electron-beam densitometer, which was described in the preceding section. The radius of a sphere was 12.4 mm.

The densitometer was installed at the window of test chamber in such a way that the electron beam can be scanned across the shock layer from the stagnation point of a sphere towards upstream (see Figure 13). The luminosity of the phosphor plate and thus the output of the photomultiplier displayed on the oscilloscope depend on the intensity of a beam arrived at the detector. As is seen from Figure 15, the beam runs without decay through gas at very low density. Therefore the initial intensity can be detected from the record for case when the flow is absent and the test chamber is sufficiently evacuated. The record for that case is shown in Figure 16. The beam location was reduced from the distance markers superimposed on the oscilloscope record. In principle the beam intensity should indicate a step-wise rise when the beam has appeared just at the stagnation point across the sphere. Since, in actual, the beam spot is of finite width, its intensity shows a steep but not step-wise at the stagnation. This will provide a limited space-resolution for the present density measurements. The estimated limit was within about ± 0.25 mm. The records of the beam intensity across the shock layer are shown in Figures 17 and 18, which are for the separate runnings of the tunnel. The respective intensity ratios I/I_0 are plotted in Figure 19, from which the mean density over the beam path can be obtained by the use of the calibration of Figure 15.

Since the flow is axisymmetric, the density is assumed to be specified as a function of only r, the distance of a point in question from the center of sphere, so far as the stagnation region is concerned. As is seen from Figure 19, the intensity ratio I/I_0 approaches a constant when proceeding upstream from

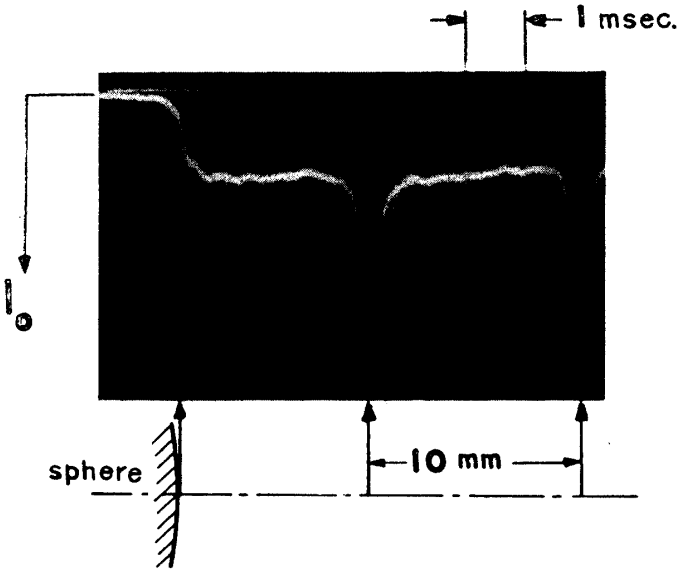

FIGURE 16. Intensity record of the scanning electron beam in case of no flow at sufficiently evacuated condition, i.e. a record of I_0.

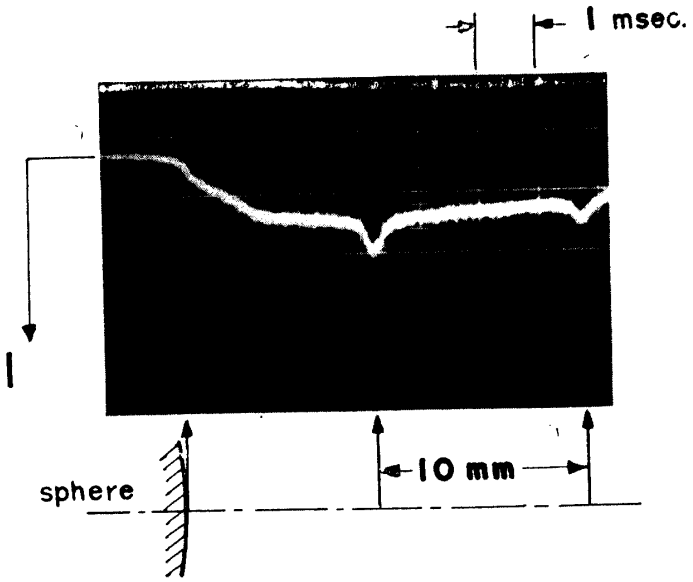

FIGURE 17. Intensity record for case when the beam was scanned across the shock layer ahead of a sphere of 12.4 mm in radius—case I.

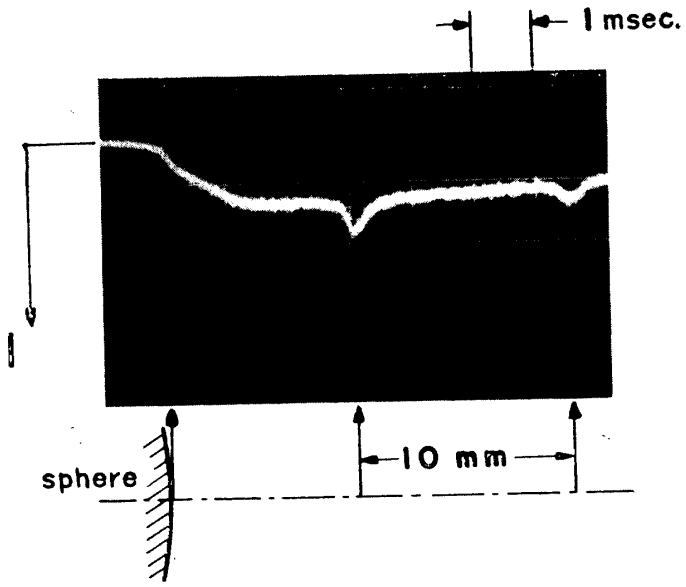

FIGURE 18. Intensity record for case when the beam was scanned across the shock laer ahead of a sphere of 12.4 mm in radius—case II.

the stagnation. This means that there exists a uniform flow upstream far from a sphere. Therefore, referring to Figure 20, one can choose a sphere of radius R, on which the density takes the free stream value ρ_∞. For a beam path across the shock layer, the local density ρ at the point where the beam intersects the stagnation line is related to the mean density $\bar{\rho}$ times the path length L, which can be obtained from the intensity ratio I/I_0, as follows:

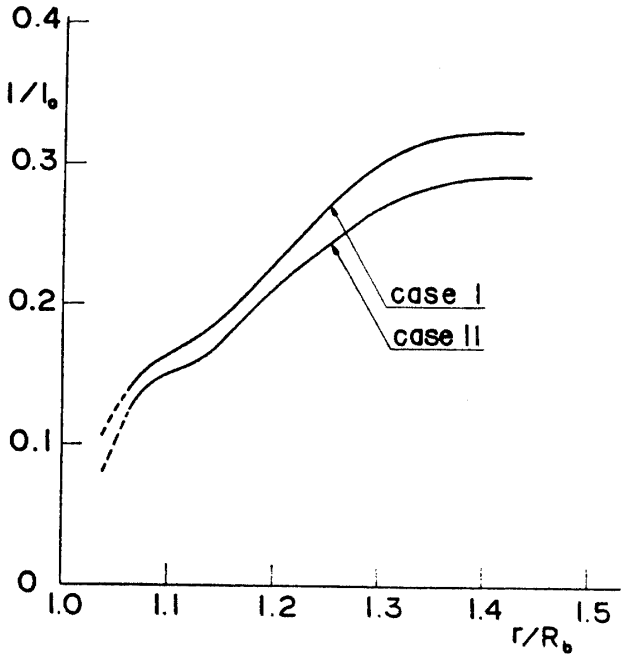

FIGURE 19. Intensity ratio I/I_0 versus r/Rb (r is distance from the stagnation and Rb the sphere radius).

$$(\bar{\rho}-\bar{\rho}_\infty)L=2\int_0^{x_\infty}\rho(r)dx-2\rho_\infty x_\infty$$
$$=2\int_0^{x_\infty}\rho^*(r)dx \qquad (6)$$

where x is the distance measured along a beam path from the stagnation line. x_∞ the x of the point where the beam intersects the sphere of radius R (see Figure 20), and

$$\rho^*=\rho-\rho_\infty$$

With y, the distance measured along the stagnation line from the center of a

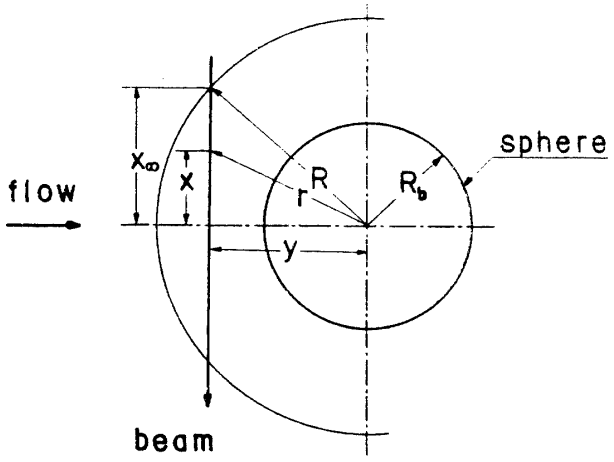

FIGURE 20. Illustrative sketch of beam path.

sphere, Eq. (6) is rewritten as

$$\Gamma \equiv (\bar{\rho}-\bar{\rho}_\infty)L = 2\int_y^R \frac{\rho^*(r)rdr}{\sqrt{r^2-y^2}} \tag{7}$$

By the transformation:

$$u^*=(y/R)^2, \quad v^*=(r/R)^2$$

Eq. (7) can be reduced to the Abel-type integral equation, so that ρ^* is given by§§

$$\rho^* = -\frac{1}{\pi R}\int_{v^*}^1 \frac{d\Gamma/du^*}{\sqrt{u^*-v^*}}\,du^*$$

The integral on the right hand side has been computed by the use of $\Gamma \equiv (\bar{\rho}-\bar{\rho}_\infty)L$, which can be obtained as a function of y/R or u^* from the beam intensity ratio. The density distribution, thus obtained, along the stagnation line is shown in Figure 21.

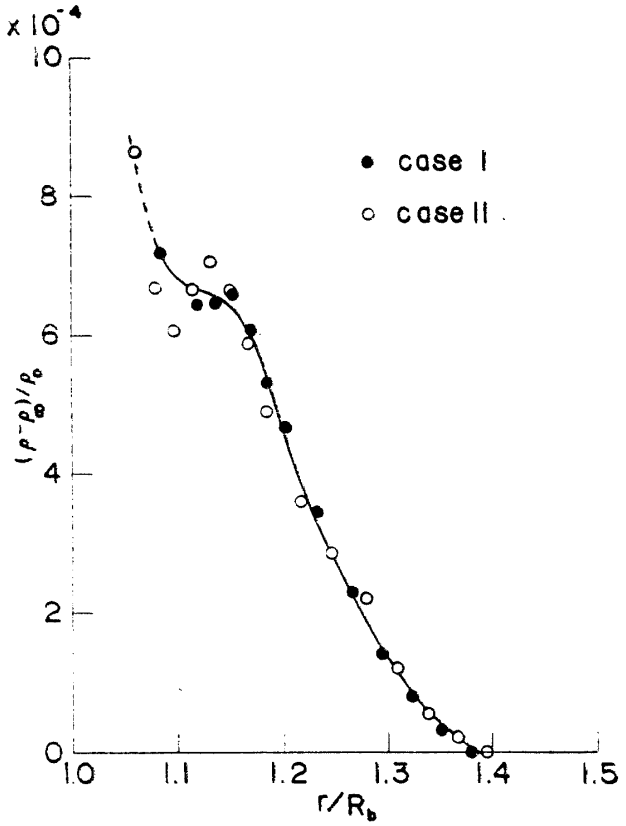

FIGURE 21. Density distribution along the stagnation line across the shock layer.

As is seen from Figure 21, the shock wave is thick but still distinguishable from the shock layer. Two kinds of plot in Figure 21 were taken from the

§§ The relation is quite similar to that between density and fringe shift in the interferometry for axisymmetric flow [9].

data of the separate runs. The test flow condition is not exactly the same from run to run. Nevertheless, the respective plots provide the quite similar profile. The density ratio ρ/ρ_∞ across the shock wave is approximately given by $(\gamma+1)/(\gamma-1)$ $(=6$ for air$)$. Therefore the free-stream density ρ_∞ is estimated from the density jump across the shock, that is

$$\rho_\infty \approx 1.3(\pm 0.1)\times 10^{-4}\rho_0$$

where ρ_0 is the density of air at NTP. The test flow condition can be determined from the isentropic relations by use of the stagnation condition and the free-stream density above estimated. The flow Mach number M and Reynolds number Re_∞, based on the sphere radius R_b were

$$M \approx 10$$

$$Re_\infty \equiv \rho_\infty u_\infty R_b/\mu_\infty \approx 650 R_b$$

or $$Re \equiv \rho_\infty u_\infty R_b/\mu_S \approx 50 R_b$$

where μ_s is the viscosity coefficient for the flow behind the shock. For the sphere applied in the present experiment, the Reynolds number is about 800.

Results and Discussion

When the Reynolds number is decreased, not only the shock layer but also the shock wave becomes thicker due to the rarefaction effects of the flow. The shock-layer structure ahead of a sphere in such a flow regime as designated as "transitional" has been analysed by Levinsky and Yoshihara [*10*] on the basis of the Navier-Stokes equations as simplified by Probstein and Kemp. [*11*] The numerical results are presented for argon $(\gamma=5/3)$ at a Mach number of 10 and Reynolds number of 10^4, 10^3 and 10^2 based on a sphere radius. To the authors' knowledge, however the experimental works concerning the shock-layer structure in a low density hypersonic flow were as yet few, while the work of Reference 12 for a cylinder at a low Mach number flow should be referred.

In the present experiment for air $(\gamma=1.4)$ the Reynolds number Re_∞ based on the sphere radius was about 800 and the free-stream Mach number 10. Since the body temperature T_b is considered the room temperature, the ratio T_b/T_0 is

$$T_b/T_0 \approx 0.3$$

In Reference 10, both limiting cases of adiabatic and cold walls were computed.

The data of Figure 21 exhibit several interesting features. It can be seen that a thick shock wave appears, its thickness being a few times the free-stream mean free path which is about 0.7 mm. In comparison with a low Mach number case of Reference 12, the density (or velocity) gradient behind the shock is much lesser than the maximum gradient within the shock, as can be expected from the fact that the density rise across the shock is much greater for higher Mach number. In the present experiment, the data for the region

close to the stagnation may be less accurate because of the limited space resolution of the densitometer, so that it leads no conclusive argument about the behavior of a viscous layer near the body. However we can see that the data show a qualitative agreement with a comparable Levinsky-Yoshihara profile, so long as the upstream region of the shock layer as well as the shock wave are concerned. It is worthwhile noting that, regardless of a difference in γ, the shock-wave location is fairly similar to that in the Levinsky-Yoshihara result for case of $Re_\infty=10^2$, in which the downstream side of the shock wave is no longer distinguishable from the shock layer.

Acknowledgement

The authors would like to express their sincere thanks to Drs. Yoshiteru Yoshinaga, Junkichi Bessho and Chihaya Ogusu of Technical Research Laboratories, NHK (Japan Broadcasting Corporation) for their helpful suggestions concerning the design and set-up of a scanning-electron-beam densitometer.

Department of Aerodynamics
Institute of Space and Aeronautical Science
University of Tokyo, Tokyo,
December 5, 1964

References

[1] H. Oguchi and K. Funabiki: Journal of Japan Aero/Space Sciences (in Japanese), **11**, 117, 26 (1963).
[2] K. N. C. Bray: In "Hypersonic Flow Research", (F. R. Riddell ed.), Progress in Astronautics and Rocketry Vol. 7, Academic Press, New York, 547 (1963).
[3] R. F. Probstein: In "Research in Heat Transfer", Pergamon Press, New York, 33 (1963).
[4] J. Rabinowicz, M. E. Jessey and C. A. Bartsch: GALCIT Hypersonic Research Project Memo. No. 33 (1956).
[5] E. Shopper and B. Schumacher: Z. Naturforsh., 8a, 700 (1951).
[6] E. M. Winkler: In "Physical Measurements in Gas Dynamics and Combustion", Princeton Univ. Press, 97 (1954).
[7] F. C. Hurlbut: J. Appl. Phys. **30**, 273 (1959).
[8] I. Wada: In "Proc. 5th Int. Symp. on Space Technology and Science", Tokyo, 251 (1963).
[9] H. Oguchi: Aero. Res. Inst., Univ. of Tokyo, Report No. 341 (1959).
[10] E. S. Levinsky and H. Yoshihara: In "Hypersonic Flow Research", (F. R. Riddell ed.), Progress in Astronautics and Rocketry Vol. 7, Academic Press, New York, 81 (1962).
[11] R. F. Probstein and N. Kemp: J. Aero/Space Sci., **27**, 174 (1960).
[12] L. Talbot and F. S. Sherman: NASA Memo. 12-14-58w (1958). Also see L. Talbot: ARS Journal **32**, 12, 1009 (1962).